High-resolution luminescence spectroscopy study of down-conversion routes in $NaGdF_4:Nd^{3+}$ and $NaGdF_4:Tm^{3+}$ using synchrotron radiation

E. van der Kolk and P. Dorenbos
Faculty of Applied Sciences, Delft University of Technology, Mekelweg 15, 2629JB Delft, The Netherlands

K. Krämer, D. Biner, and H. U. Güdel
Department of Chemistry and Biochemistry, University of Bern, Freiestrasse 3, 3000 Bern 9, Switzerland
(Received 2 August 2007; published 10 March 2008)

Down-conversion in lanthanide doped luminescent materials is a promising route to significantly enhance the energy efficiency of silicon solar cells, plasma display panels, or mercury-free lighting tubes because it results in the emission of two photons for each absorbed higher energy photon. The Gd^{3+}/Eu^{3+} ion couple shows down-conversion of vacuum-ultraviolet light into visible light with an efficiency close to 190%. The low absorption strength of the $^6G_{7/2}$ levels of Gd^{3+} (the starting point of the down-conversion process), however, prevents efficient excitation of the down-conversion process and therefore application. We have performed a high resolution luminescence spectroscopy study, using synchrotron radiation, in order to investigate the possibility to use the strong $4f \rightarrow 5d$ absorption transitions of Nd^{3+} and Tm^{3+} to sensitize the high energy $^6G_{7/2}$ level of Gd^{3+} in the phosphors $NaGdF_4:2\%Nd^{3+}$ and $NaGdF_4:2\%Tm^{3+}$. Tm^{3+} appears to be an efficient sensitizer of the $^6G_{7/2}$ state of Gd^{3+}. It was also found that sensitization is followed by two successive energy transfer processes exciting two Tm^{3+} ions in the $^3H_4$ state which results in the emission of two infrared photons for one absorbed vacuum-ultraviolet photon. Nd^{3+} is not a good sensitizer of the $^6G_{7/2}$ state in $NaGdF_4$. Instead Nd^{3+} efficiently transfers its energy by cross relaxation to the lower energy ^6D_J states of Gd^{3+} but leaving the Nd^{3+} ion excited in the $^4F_{3/2}$ state. Successive energy transfer from Gd^{3+} back to Nd^{3+} excites a second Nd^{3+} ion in the $^4F_{3/2}$ state. Also, in this case, two infrared photons can be emitted for one absorbed vacuum-ultraviolet photon.

DOI: 10.1103/PhysRevB.77.125110 PACS number(s): 78.40.Ha, 71.70.Gm, 78.47.−p, 78.55.Hx

I. INTRODUCTION

There is a real need for luminescent materials that emit two visible or infrared (IR) photons for each absorbed vacuum-ultraviolet (VUV) or ultraviolet (UV) photon. Such quantum cutting (or quantum splitting) phosphors can be applied in plasma display panels (PDPs), Hg-free lighting tubes, or solar cells to raise energy efficiency.[1–4]

In PDPs and Hg-free lighting, phosphors are applied, which need to convert high energy VUV light from a noble gas discharge (between 7 and 9 eV) into visible red, green, and blue lights (1.7–3 eV).[5] Although the quantum efficiency of currently applied conventional phosphors is close to the possible maximum (100%),[6] the energy efficiency is rather low due to the large difference between the excitation and emission energies. Application of quantum cutting phosphors can, in principle, raise the energy efficiency by a factor of 2.[1]

Silicon solar cells hamper with a very similar problem. Although the UV and visible part of the solar spectrum is efficiently absorbed by silicon, the excitation energy in excess of the silicon band gap that is about 1.2 eV is lost by thermalization. It has been calculated that in the ideal case, a quantum cutting luminescent material converting UV and visible light into IR light can enhance the energy efficiency of a solar cell from 29% to 37%.[4]

The phenomena of quantum cutting can be achieved by an energy relaxation mechanisms generally referred to as down-conversion. Wegh *et al.*[1] discovered a promising phosphor $LiGdF_4:Eu^{3+}$, in which down-conversion is achieved by a two step energy transfer process between two different lanthanide ions Gd^{3+} and Eu^{3+} (see Fig. 1). After a Gd^{3+} ion has been excited into the high energy $^6G_{7/2}$ state, cross relaxation occurs between Gd^{3+} and Eu^{3+} (dashed arrows) resulting in an excited Eu^{3+} ion ready to emit a red photon. Cross relaxation is followed by a second energy transfer step from Gd^{3+} (curved arrow) that excites a second Eu^{3+} ion that will emit a

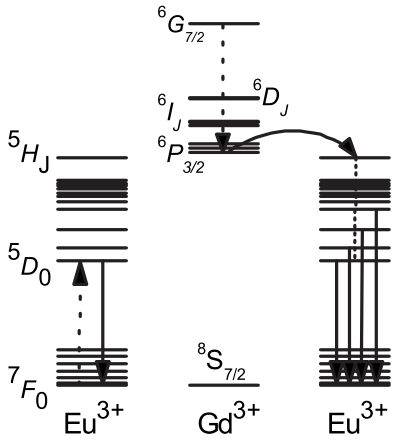

FIG. 1. Schematic energy level diagram of Gd^{3+} and Eu^{3+} in $LiGdF_4$. The observed quantum splitting process by down-conversion involving cross relaxation (dashed arrows), energy transfer (curved arrow), and multiphonon relaxation (dotted arrow) leads to the emission of two red photons by Eu^{3+} (solid arrows) for each Gd^{3+} ion that is excited in its $^6G_{7/2}$ state. Note that for clarity, not all energy levels are shown.

second red photon. The quantum efficiency of $LiGdF_4:Eu^{3+}$ was reported to be close to 190%.[1]

A drawback of this phosphor is the low absorption efficiency into the high energy $^6G_{7/2}$ state of Gd^{3+}. The absorption transition is spin and parity forbidden and, therefore, weak. These problems were emphasized by Feldmann *et al.*[7] who showed that the external quantum efficiency, a more practical quantity that also takes into account the absorption efficiency of $LiGdF_4:Eu^{3+}$, was only 32%. Clearly, the sensitization of high energy $^6G_{7/2}$ state of Gd^{3+} is of crucial importance.

Several reports can be found in literature on the sensitization of Gd^{3+} by other ions with high absorption cross section and efficient energy transfers to the $^6G_{7/2}$ state of Gd^{3+}. Babin *et al.*[8] considered the role of Pb^{2+} as a sensitizer for the $^6G_{7/2}$ state of Gd^{3+}. Peijzel *et al.*[9] successfully used Tm^{3+} as a sensitizer in $LiGdF_4:Eu^{3+},Tm^{3+}$ but discovered at the same time that the cross-relaxation step from Gd^{3+} to Eu^{3+}, described above Fig. 1, was quenched by more efficient cross relaxation from Gd^{3+} to Tm^{3+}. A similar competing cross relaxation from Gd^{3+} to Nd^{3+} was found by Jia *et al.* in $LiGdF_4:Nd^{3+}$.[10]

In this work, the ions Nd^{3+} and Tm^{3+} in hexagonal $NaGdF_4$ are investigated as potential sensitizers for the high energy Gd^{3+} $^6G_{7/2}$ state. In $NaGdF_4$, both ions have $5d$ states at higher energies than the Gd^{3+} $^6G_{7/2}$ state which makes energy transfer energetically possible. They also have no $4f$ levels close in energy below the $5d$ states, which makes a nonradiative relaxation from the $5d$ states to the $4f$ states of Tm^{3+} or Nd^{3+} improbable. In addition, these ions are expected to have $5d \rightarrow 4f$ emission bands that spectrally overlap with the Gd^{3+} ^6G_J states, which makes a resonant energy transfer from Nd^{3+} or Tm^{3+} to Gd^{3+} possible.

The host material $NaGdF_4$ is a member of the hexagonal $NaLnF_4$ family (Ln=Y,La-Lu). Its structure was first determined for $NaNdF_4$,[11] and its Na^+/Ln^{3+} disorder was recently refined for $NaLaF_4$ and $NaGdF_4$.[12] Due to its cation disorder, the two slightly different Ln^{3+} sites and the short Ln-Ln distances of two times 3.61 Å and six times 3.92 Å for the example of $NaGdF_4$, it is the most efficient up-conversion host lattice[13] hitter to known. Thus, strong Ln-Ln interactions are expected for $NaGdF_4:Nd^{3+}$ and Tm^{3+} compounds, too.

This paper is organized as follows. First, experimental results on single doped $NaLaF_4:2\%Nd^{3+}$ are presented to establish the dominant emission characteristics of Nd^{3+} in this host. Second, the energy transfer mechanisms from Nd^{3+} to Gd^{3+} are investigated in hexagonal $NaGdF_4:Nd^{3+}$, and conclusions are drawn about the sensitizing potential of Nd^{3+}. Third, the focus will be on a possible energy back transfer from Gd^{3+} to Nd^{3+}. Finally, the same investigations are presented and discussed for Tm^{3+} in hexagonal $NaGdF_4$.

II. EXPERIMENTAL PROCEDURES

A. Materials synthesis

Powder samples of phase-pure hexagonal $NaLaF_4:2\%M^{3+}$ and $NaGdF_4:2\%M^{3+}$ (M=Nd or Tm) fluorides were prepared from rare-earth oxides Re_2O_3 (Re=La, Nd, Gd, and Tm) of 5N or 6N purity (Metal Rare Earth Ltd.), Na_2CO_3 (Alfa, 5N), and aqueous 65% HNO_3 (Merck, p.a.) and 40% HF acids (Merck, supra pure). Batches were typically calculated for 5 g of product. The stoichiometric mixture of the respective rare-earth oxides was dissolved in a small amount of HNO_3 in a Teflon beaker, evaporated to dryness, dissolved in water, and the fluorides MF_3 precipitated with HF. The liquid is evaporated and HF is added again. For the work with HF acid or gas, appropriate safety precautions have to be taken. The respective amount of Na_2CO_3 to obtain a 2:1 ratio of Na to M is dissolved in water in a separate beaker and slowly added to the mixture. Care has to be taken to avoid spilling due to the CO_2 evolution. The product is dried, and the addition of HF and drying are repeated. The solid, which consists of a mixture of MF_3 and NaF according to x-ray diffraction, is ground up in a mortar, transferred into a glassy carbon boat, and heated to 550 °C in a HF/Ar gas stream for 20 h. The sample is heated in a tubular furnace in a gas tight nickel apparatus (alloy 600) which is inert to HF gas. In this step, the reaction toward hexagonal $NaMF_4$ plus excess NaF takes place. Traces of O are removed by the HF gas stream. The powder is ground up again and heated to 590 °C in an Ar gas stream for another 20 h. This step improves the crystallinity and optical properties of the material. Finally, the product is washed with water to dissolve the excess NaF and then dried at 100 °C. All samples were checked by x-ray powder diffraction. They show the hexagonal $NaLaF_4$ phase[12,13] together with a small residue of about 0.5% NaF.

B. Spectroscopic measurements

Luminescence excitation spectra were recorded at the Deutsche Electronen-Synchrotron (DESY) in Hamburg (Germany) using the SUPERLUMI station of HASYLAB. The spectral region of excitation was 50–335 nm with a fixed resolution of 0.3 nm. A R6358P Hamamatsu photomultiplier tube (PMT) connected to a triple grating Czerny-Turner monochromator SpectraPro-308i from Acton Research, Inc., was used to measure excitation spectra of UV to visible luminescence. All excitation spectra were corrected for the wavelength dependent excitation intensity. Details of this excitation facility were described elsewhere.[14]

Luminescence emission spectra were recorded with a liquid nitrogen cooled charge coupled device (CCD) detector of Princeton Instruments, Inc., connected to the monochromator described above. The sensitive spectral range was between 200 and 1100 nm with a resolution close to 1 nm. All emission spectra were corrected for the wavelength dependent detection efficiency. Time resolved emission spectra were recorded with a fast PMT connected to the same monochromator by setting a desired time window (gate) after pulsed synchrotron excitation. All presented data were recorded at 10 K.

III. EXPERIMENTAL RESULTS AND DISCUSSION

A. Vacuum-ultraviolet spectroscopy of $NaLaF_4:2\%Nd^{3+}$

Figure 2 combines the emission spectrum of $NaLaF_4:Nd^{3+}$ under excitation at 156 nm [curve (b)] and the

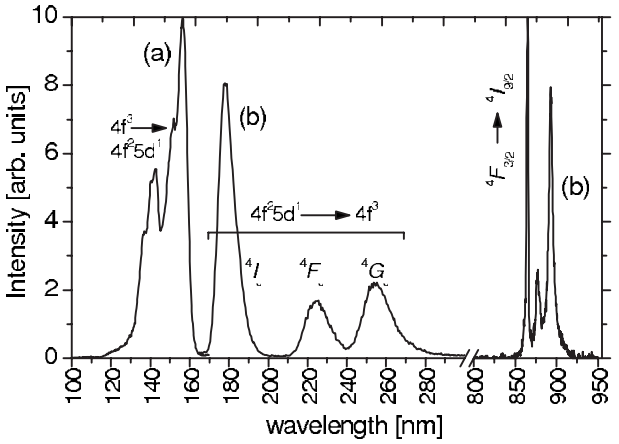

FIG. 2. (a) Excitation spectrum of $NaLaF_4:2\%Nd^{3+}$ monitoring the Nd^{3+} $4f^25d^1 \rightarrow 4f^3$ emission at 178 nm. (b) Emission spectrum of $NaLaF_4:2\%Nd^{3+}$ excited in the $4f^25d^1$ states of Nd^{3+} at 156 nm. Both spectra were recorded at 10 K.

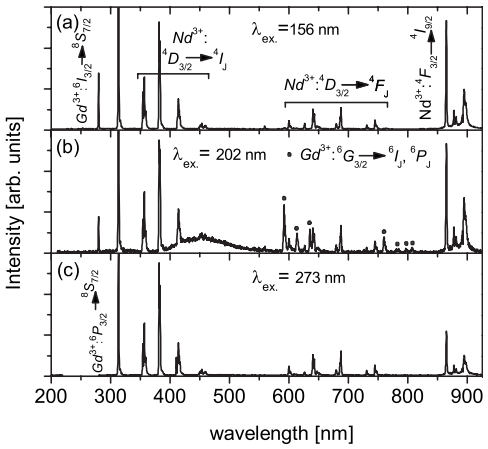

FIG. 4. Emission spectra of $NaGdF_4:2\%Nd^{3+}$ recorded at 10 K during (a) Nd^{3+} $4f^25d^1 \rightarrow 4f^3$ excitation at 156 nm, (b) Gd^{3+} $^8S_{7/2} \rightarrow {}^6G_J$ excitation at 202 nm, and (c) Gd^{3+} $^8S_{7/2} \rightarrow {}^6I_J$ excitation at 273 nm. The three spectra were normalized at the Nd^{3+} $^4D_{3/2} \rightarrow {}^4I_{9/2}$ transition at 383 nm.

excitation spectrum (curve a) monitoring the Nd^{3+} emission at 178 nm. The excitation spectrum shows bands between 130 and 160 nm corresponding to the $4f^25d^1$ configuration of Nd^{3+}. The emission spectrum consists of both $4f^25d^1 \rightarrow 4f^3$ [^4I_J, ^4F_J, ^4G_J] emissions at 178, 225, and 255 nm respectively, and $4f^3 \rightarrow 4f^3$ emission around 875 nm corresponding to the Nd^{3+} $^4F_{3/2} \rightarrow {}^4I_{9/2}$ transition. The ratio between $5d \rightarrow 4f$ and $4f \rightarrow 4f$ emissions upon Nd^{3+} $5d$ excitation is controlled to a large extent by the energy gap between the Stokes shifted lowest energy $5d$ state and the first lower energy $4f^3$ state. Only when this gap is small enough [typically <7500 cm^{-1} (Ref. 15)], nonradiative feeding of the $^2G_{9/2}$ level of Nd^{3+} (around 48.000 cm^{-1}) is possible. Under these conditions, a large number of $4f^3 \rightarrow 4f^3$ emission lines in the UV and visible spectral range are observed.[15] Since only very weak $4f^3 \rightarrow 4f^3$ emission lines are observed in $NaLaF_4:Nd^{3+}$, it must be concluded that $5d \rightarrow 4f$ emission is the dominant relaxation route after Nd^{3+} $4f \rightarrow 5d$ excitation. The observed $^4F_{3/2} \rightarrow {}^4I_{9/2}$ emission around 875 nm is the result of radiative feeding of the ^4G_J (255 nm) and the ^4F_J (225 nm) states, as indicated in Fig. 3(a).

B. Down-conversion in $NaGdF_4:2\%Nd^{3+}$

The emission spectrum of $NaGdF_4:Nd^{3+}$ under Nd^{3+} $4f^25d^1$ excitation at 156 nm is plotted in Fig. 4(a). When this emission spectrum is compared with the emission spectrum of $NaLaF_4:Nd^{3+}$, also excited at 156 nm (Fig. 2), it can be observed that the Nd^{3+} $5d \rightarrow 4f$ emission is completely quenched in $NaGdF_4:Nd^{3+}$. Instead, Gd^{3+} emission from the $^6P_{3/2}$ and the $^6I_{3/2}$ levels to the $^8S_{7/2}$ ground state is observed at 279 and 313 nm, respectively, as well as emission from the $^4D_{3/2}$ and $^4F_{3/2}$ levels of Nd^{3+} [see Fig. 4(a)]. Clearly, energy is transferred completely from the $5d$ states of Nd^{3+} to the $4f$ levels of Gd^{3+}. Figure 4(b) represents the emission spectrum of $NaGdF_4:Nd^{3+}$ under direct Gd^{3+} excitation into a ^6G_J level at 202 nm. At this excitation wavelength, emission from the $^6G_{7/2}$ Gd^{3+} level is observed, as indicated by the black dots. Since these emissions were not observed under Nd^{3+} $5d$ excitation, it must be concluded that energy transfer from Nd^{3+} to Gd^{3+} proceeds to any of the lower energy ^6D_J, ^6I_J, and ^6P_J states of Gd^{3+} and not the ^6G_J states.

This energy transfer route is confirmed by the excitation spectra plotted in Fig. 5 monitoring the Gd^{3+} $^6G_{7/2} \rightarrow {}^6P_{3/2}$ emission at 592 nm [spectrum (a)] and the Gd^{3+} $^6P_{3/2} \rightarrow {}^8S_{7/2}$ emission at 313 nm [spectrum (b)]. Spectrum (a) directly proves that $^6G_{7/2}$ emission at 592 nm can only be excited into the ^6G_J levels themselves but not into the Nd^{3+} $5d$ states. Spectrum (b) confirms that the Gd^{3+} $^6P_{3/2} \rightarrow {}^8S_{7/2}$ emission at 311 nm is sensitized by the Nd^{3+} $5d$ states.

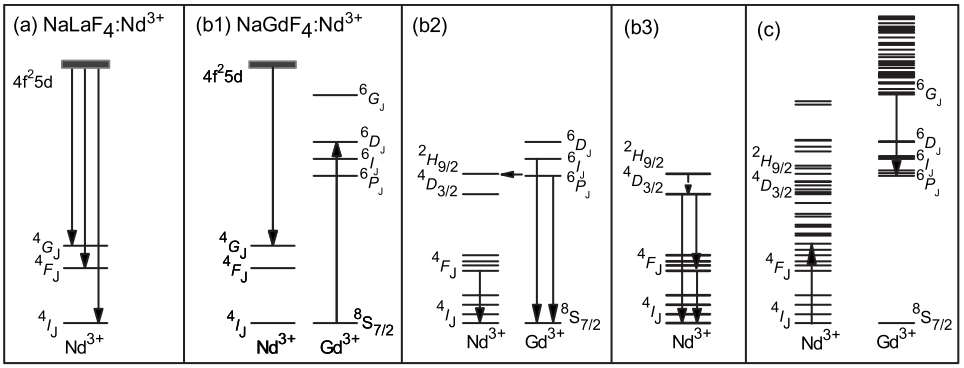

FIG. 3. Schematic energy level diagrams of Nd^{3+} and Gd^{3+} in (a) $NaLaF_4:2\%Nd^{3+}$ and [(b) and (c)] $NaGdF_4:Nd^{3+}$ showing the observed radiative and energy transfer relaxation routes after optical excitation of the [(b1)–(b3)] Nd^{3+} $5d$ state and the (c) ^6G_J states of Gd^{3+}. Note that only relevant energy levels are shown.

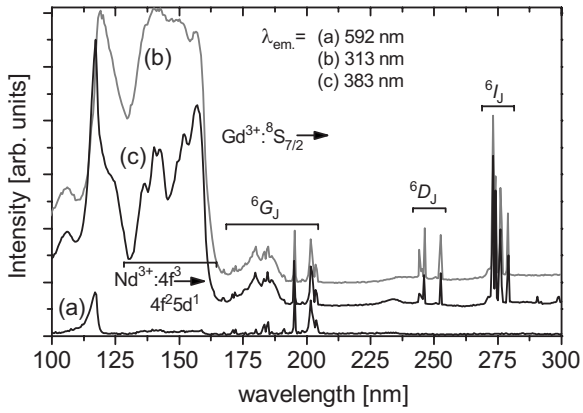

FIG. 5. Excitation spectra of $NaGdF_4:2\%Nd^{3+}$ recorded at 10 K monitoring (a) the Gd^{3+} $^6G_{7/2}\rightarrow{}^6P_{3/2}$ transition at 592 nm, (b) the Gd^{3+} $^6P_{3/2}\rightarrow{}^8S_{7/2}$ transition at 313 nm, and (c) the Nd^{3+} $^4D_{3/2}\rightarrow{}^4I_{9/2}$ transition at 383 nm.

The selective energy transfer from the $5d$ states of Nd^{3+} to the lower energy states of Gd^{3+} can be explained by a favorable spectral overlap between the lower energy ^6D_J, ^6I_J, and ^6P_J states of Gd^{3+} and the $4f^25d^1\rightarrow4f^3$ emission bands of Nd^{3+}. Figures 6(a) and 6(b), representing the Nd^{3+} $5d\rightarrow4f$ emission and the Gd^{3+} $4f\rightarrow4f$ excitation spectrum, respectively, indeed confirm a good spectral overlap around 255 nm between Nd^{3+} $4f^25d^1\rightarrow4f^3[^4G_J]$ emission and Gd^{3+} $^8S_{7/2}\rightarrow{}^6D_J$ absorption. Figure 3(b1) shows the identified cross-relaxation process in $NaGdF_4:Nd^{3+}$ that explains the selective energy transfer from Nd^{3+} to Gd^{3+}.

Jia *et al.*[10] recently studied sensitization of Gd^{3+} by Nd^{3+} in $LiGdF_4:Nd^{3+}$ and assumed a cross-relaxation process from the $5d$ states of Nd^{3+} to the higher energy ^6G_J levels of Gd^{3+}. They, however, at the same time, noted that cross relaxation to the lower lying ^6D_J, ^6I_J, and ^6P_J states of Gd^{3+}

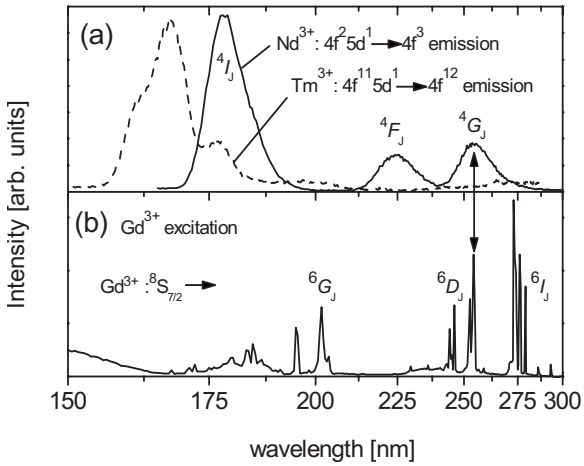

FIG. 6. Spectral energy overlap between the Nd^{3+} and Tm^{3+} $5d\rightarrow4f$ emission and Gd^{3+} $4f\rightarrow4f$ excitation in $NaGdF_4:2\%Nd^{3+}$ and $NaGdF_4:2\%Tm^{3+}$, respectively. (a) Nd^{3+} emission spectrum (solid) recorded at 10 K under $4f^3\rightarrow4f^25d$ excitation at 156 nm and the Tm^{3+} emission spectrum (dashed) under $4f^{12}\rightarrow4f^{11}5d$ excitation at 131 nm. (b) Excitation spectrum recorded at 10 K monitoring the Gd^{3+} $^6P_{3/2}\rightarrow{}^8S_{7/2}$ transition at 313 nm.

could not be excluded on the bases of their experimental data. Our data clearly show that in $NaGdF_4:Nd^{3+}$, the lower energy Gd^{3+} levels are sensitized by the $5d$ states of Nd^{3+}. Our conclusion is based on the excitation spectrum monitoring Gd^{3+} $^6G_{7/2}$ emission that shows no Nd^{3+} $5d$ excited states [see Fig. 5(a)] and the favorable spectral overlap between the $5d\rightarrow4f$ Nd^{3+} emission and the Gd^{3+} $^8S_{7/2}\rightarrow{}^6D_J$ absorption (Fig. 6). Because no emission from the $^6G_{7/2}$ level of Gd^{3+} was observed in $LiGdF_4:Nd^{3+}$, a simple proof as was given in this work cannot be given. The emission of Nd^{3+} in $LiGdF_4$ is, however, expected to be the same as in $LiYF_4:Nd^{3+}$ (Ref. 10) which, in turn, is the same as in $NaGdF_4:Nd^{3+}$ (compare Ref. 16 and Fig. 6 of this work). Spectral overlap between Nd^{3+} emission and Gd^{3+} absorption in $LiGdF_4:Nd^{3+}$ will therefore be the same as in $NaGdF_4$ which suggests that sensitization of the high energy ^6G_J levels does not take place in $LiGdF_4:Nd^{3+}$.

The emission from the $^4D_{3/2}$ state of Nd^{3+} [see Fig. 4(a)], which is observed under Nd^{3+} $5d$ excitation, is the result of a partial energy transfer from the $^6P_{3/2}$ level of Gd^{3+} to Nd^{3+}, as indicated by the vertical arrow in Fig. 3(b2). This transfer is demonstrated by the observation of Nd^{3+} $^4D_{3/2}$ emissions under direct Gd^{3+} $^8S_{7/2}\rightarrow{}^6I_J$ excitation at 273 nm [see Fig. 4(c)]. In addition, excitation spectrum (c) plotted in Fig. 5, monitoring the Nd^{3+} $^4D_{3/2}\rightarrow{}^4I_{9/2}$ emission at 383 nm, clearly reveals the Gd^{3+}: $^8S_{3/2}\rightarrow{}^6P_J$, ^6I_J, and ^6G_J transitions, which confirms the $Gd^{3+}\rightarrow Nd^{3+}$ back transfer.

The above described down-conversion process involving a two step energy transfer process from Nd^{3+} to Gd^{3+} [step 1, Fig. 3(b1)] and back from Gd^{3+} to Nd^{3+} [step 2, Fig. 3(b2)] can result in the emission of two IR photons by Nd^{3+} ($^4F_{3/2}\rightarrow{}^4I_{9/2}$) for each absorbed VUV photon (between 130 and 160 nm). The first cross-relaxation step [Fig. 3(b1)] populates the Nd^{3+} $^4F_{3/2}$ state and the Gd^{3+} $^6D_{9/2}$ state. Subsequently, the back-transfer step discussed above [Fig. 3(b2)] populates the Nd^{3+} $^4D_{3/2}$ levels. Finally, the Nd^{3+} $^4F_{3/2}$ state is populated the second time by Nd^{3+} $^4D_{3/2}\rightarrow{}^4F_J$ emission [Fig. 3(b3)]. Further experimental evidence for this down-conversion process can be found by comparing the emission spectra plotted in Figs. 4(a) and 4(c) that are both normalized at 383 nm, i.e., the Nd^{3+} $^4D_{3/2}\rightarrow{}^4I_{7/2}$ emission line. The enhanced IR emission (around 875 nm) under Nd^{3+} $5d$ excitation [Fig. 4(a)] compared to direct Gd^{3+} ^6I_J excitation [Fig. 4(c)] is the expected consequence of the down-conversion process described above. Note that, although with poor quantum efficiency, there is a change for emission of three photons for an absorbed VUV photon, i.e., two times $^4F_{3/2}\rightarrow{}^4I_{9/2}$ and one times $^4D_{3/2}\rightarrow{}^4F_J$.

Finally, it is interesting to note that the emission spectrum obtained under direct Gd^{3+} ^6G_J excitation at 202 nm, shown in Fig. 4(b), also shows enhanced IR emission compared to ^6I_J excitation at 273 nm [Fig. 4(c)]. This can be explained by down-conversion involving a two step energy transfer process from the $^6G_{7/2}$ level of Gd^{3+} to the $^4F_{3/2}$ level of Nd^{3+} that was described earlier by Jia *et al.*[10] for $LiGdF_4:Nd^{3+}$. The first step is cross relaxation involving the Gd^{3+} [$^6G_{3/2}\rightarrow{}^6P_J$] and the Nd^{3+} [$^4I_{9/2}\rightarrow{}^4F_J$] transitions, as indicated by the vertical arrows in Fig. 3(c), resulting in excitation of the Nd^{3+} $^4F_{3/2}$ state and excitation of the Gd^{3+} $^6P_{3/2}$ state. The

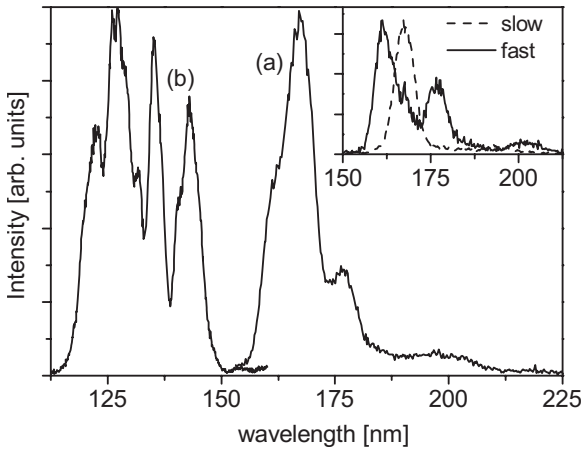

FIG. 7. (a) Excitation spectrum of $NaLaF_4:2\%Tm^{3+}$ recorded at 10 K monitoring the Tm^{3+} $4f^{11}5d^1 \rightarrow 4f^{12}$ emission at 176 nm. (b) Emission spectrum recorded at 10 K excited in the $4f^{11}5d^1$ states of Tm^{3+} at 131 nm. The inset shows time resolved emission spectra recorded after pulsed synchrotron excitation between 2 and 10 ns ("fast") and 80 and 160 ns ("slow").

second step is the previously described back transfer process resulting in excitation of a second Nd^{3+} ion into the $^4F_{3/2}$ state [see Figs. 3(b2) and 3(b3)].

From an application point of view, it must be noted that the overall internal quantum efficiency for Nd^{3+} $^4F_{3/2}$ emission in $NaGdF_4:Nd^{3+}$ under $Nd^{3+}5d$ excitation or direct Gd^{3+} excitation is low because the Gd^{3+} $^6P_{3/2} \rightarrow {}^8S_{7/2}$ and the Nd^{3+} $^4D_{3/2} \rightarrow {}^4I_J$ emissions contain most of the intensity. In addition, the enhanced Nd^{3+} $^4F_{3/2}$ emission is located in the IR which is useless for lamp or display applications.

C. Vacuum-ultraviolet spectroscopy of $NaLaF_4:2\%Tm^{3+}$

Figure 7 shows the emission spectrum [trace (a)] of $NaLaF_4:Tm^{3+}$ recorded during Tm^{3+} $4f \rightarrow 5d$ excitation at 131 nm and the excitation spectrum [trace (b)] monitoring Tm^{3+} $5d \rightarrow 4f$ emission at 176 nm. Unique identification of the $5d \rightarrow 4f$ emission bands of Tm^{3+} is possible by studying

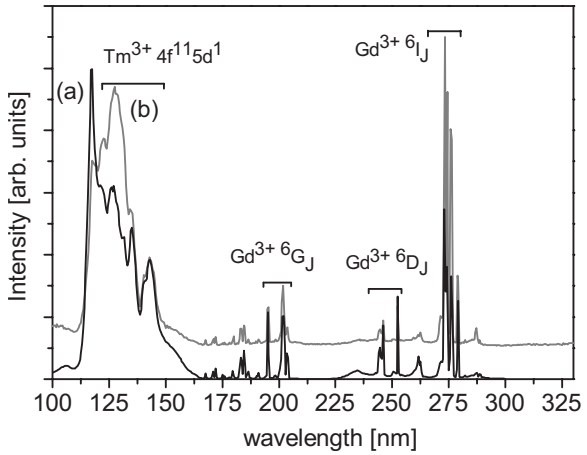

FIG. 8. Excitation spectra of $NaGdF_4:2\%Tm^{3+}$ recorded at 10 K monitoring (a) the Gd^{3+} $^6P_{3/2} \rightarrow {}^8S_{7/2}$ emission at 313 nm and (b) the Tm^{3+} $^3P_0 \rightarrow {}^3H_4$ emission at 345 nm.

the time resolved emission spectra plotted in the inset of Fig. 7. The fast component of the emission (solid curve) was recorded between 3 and 10 ns after pulsed synchrotron excitation. The slow component (dashed curve) was recorded between 60 and 180 ns. The emission spectrum is composed of two emission bands at 161.6 and 176.8 nm with a short decay time, which correspond to the spin-allowed $5d \rightarrow 4f$ transition starting from the high spin $5d$ state of Tm^{3+} (Ref. 16) to the $^3F_4$ and $^3H_6$ states. Another emission band at 167.5 nm with a longer decay time corresponds to the spin-forbidden $5d \rightarrow 4f$ transition starting from the low spin $5d$ state of Tm^{3+} (Ref. 17) to the $^3H_6$ state. These transitions are indicated in Fig. 10(a). The excitation spectrum monitoring both the spin allowed and spin forbidden $5d \rightarrow 4f$ transitions around 177 nm, shown in Fig. 7 [trace (b)], consists of $4f \rightarrow 5d$ excitation bands of Tm^{3+} between 120 and 150 nm.

D. Down-conversion in $NaGdF_4:2\%Tm^{3+}$

Figure 8(a) shows the excitation spectrum of $NaGdF_4:Tm^{3+}$ monitoring Gd^{3+} emission at 313 nm. Besides the expected Gd^{3+} $4f^7$ lines, the spectrum contains the same broad band features that were observed in the excitation spectra of $NaLaF_4:2\%Tm^{3+}$ monitoring Tm^{3+} $5d \rightarrow 4f$ emission and are therefore assigned to the $5d$ states of Tm^{3+}. This excitation spectrum therefore proves energy transfer from the $5d$ states of Tm^{3+} to the $4f$ states of Gd^{3+}. The emission spectrum of $NaGdF_4:Tm^{3+}$ recorded under Tm^{3+} $5d$ excitation at 143 nm is plotted in Fig. 9(a). It is dominated by Gd^{3+} $^6P_{3/2} \rightarrow {}^8S_{7/2}$ emission at 313 nm which confirms efficient energy transfer from Tm^{3+} to Gd^{3+}.

In Fig. 6, the Tm^{3+} $5d \rightarrow 4f$ emission spectrum is compared with the Gd^{3+} excitation spectrum. It shows that the $5d \rightarrow 4f$ emission only has spectral overlap with the ^6G_J states of Gd^{3+}. Contrary to the situation for $NaGdF_4:Nd^{3+}$, there is no $5d \rightarrow 4f$ emission overlapping with the lower energy ^6D_J, ^6I_J, and ^6P_J states of Gd^{3+}. This strongly suggests that energy is transferred from the $5d$ states of Tm^{3+} to the ^6G_J state of Gd^{3+}, as indicated by the curved arrows in

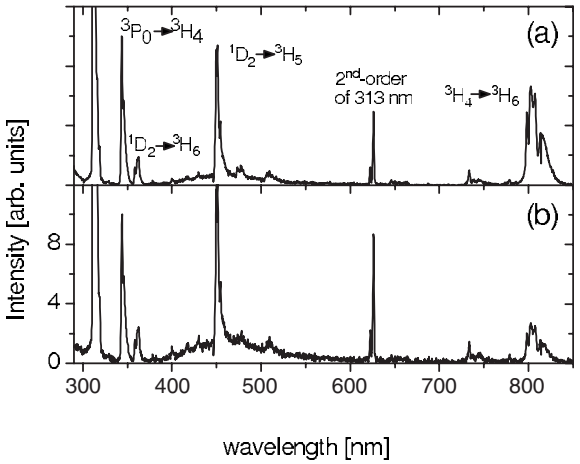

FIG. 9. Emission spectra of $NaGdF_4:2\%Tm^{3+}$ recorded at 10 K during (a) Tm^{3+} $4f^{12} \rightarrow 4f^{11}5d^1$ excitation at 143 nm and (b) Gd^{3+} $^8S_{7/2} \rightarrow {}^6D_J$ excitation at 252 nm. The two spectra were normalized at the $^3P_0 \rightarrow {}^3H_4$ transition.

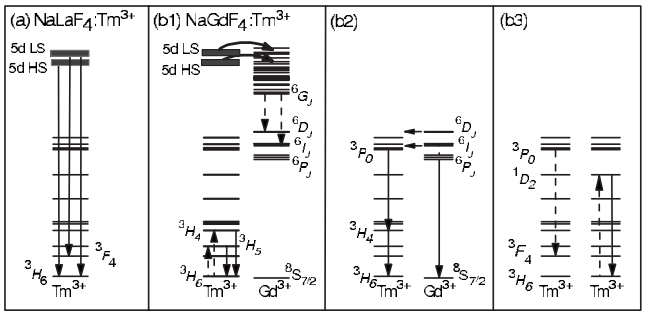

FIG. 10. Schematic energy level diagram of Tm^{3+} in $NaLaF_4$ and the observed spin-allowed and spin-forbidden $4f^{11}5d^1 \rightarrow 4f^{12}$ transitions. (b) Energy level diagram of Tm^{3+} and Gd^{3+} in $NaGdF_4$:2% Tm^{3+} showing the observed radiative and energy transfer relaxation routes after optical excitation of (b1)–(b3) the $5d$ state of Tm^{3+}. Note that for clarity, not all energy levels have been drawn.

Fig. 10(b1). The same type of transfer was observed in $LiGdF_4$:Tm^{3+} by Peijzel *et al.*[9]

Figure 9(a) shows no evidence of emission from $^6G_{3/2}$ state of Gd^{3+}. Instead, it shows strong Gd^{3+} $^6P_{3/2}$ emission at 313 nm and emission from the Tm^{3+} $^3H_4$ state around 800 nm. Since there is no direct transfer route from the $5d$ states of Tm^{3+} to the Gd^{3+} $^6P_{3/2}$ state, and no Gd^{3+} $^6G_{3/2}$ emission is observed, there must be an efficient cross relaxation between Tm^{3+} and Gd^{3+}. The most likely cross-relaxation route that was also adopted by Peijzel *et al.* for $LiGdF_4$:Tm^{3+} is indicated by the dashed arrows in Fig. 10(b1). Cross relaxation involves the transitions $^6G_{3/2} \rightarrow {}^6I_J$, ^6D_J on Gd^{3+} and $^3H_4 \rightarrow {}^3H_6$, $^3H_5$ on Tm^{3+} and thus explains not only the emission from the $^6P_{3/2}$ state of Gd^{3+} (after nonradiative relaxation from the ^6I_J, ^6D_J states) upon Tm^{3+} $5d$ excitation but also the emission from the $^3H_4$ state of Tm^{3+}.

Figure 8(b) shows the excitation spectrum of $NaGdF_4$:2% Tm^{3+} monitoring the Tm^{3+} $^3P_0 \rightarrow {}^3H_4$ emission at 345 nm. The spectrum shows that Tm^{3+} $^3P_0$ emission can be excited into the ^6G_J, ^6D_J, and ^6I_J states of Gd^{3+} but not in the ^6P_J states. This is explained by the energy level diagrams of Gd^{3+} and Tm^{3+} [see Fig. 10(b2)], which show no possibility for energy transfer from Gd^{3+} ^6P_J state to the Tm^{3+} $^3P_0$ state because it is located at a too low energy. This explains the high intensity of the Gd^{3+} $^6P_{3/2}$ emission. The observed $^3P_0$ emission must therefore be the result of transfer from the $^6I_{3/2}$ and $^6D_{3/2}$ states of Gd^{3+}, as indicated by the horizontal arrows in Fig. 10(b2).

The emission from the $^1D_2$ state observed under Tm^{3+} $5d$ excitation cannot be explained by nonradiative $4f \rightarrow 4f$ relaxation from the $^3P_0$ state to the $^1D_2$ state given the large energy gap and the low phonon energy characteristic of the $NaGdF_4$ host. A radiative feeding from the excited Tm^{3+} $5d$ state can also be excluded since no corresponding emission is observed. $^1D_2$ emission is therefore explained by cross relaxation between nearest neighbor Tm^{3+} ions, as indicated by the dashed arrows in Fig. 10(b3).

In Fig. 9(a), the Tm^{3+} $4f^{12} \rightarrow 4f^{11}5d^1$ transition is excited at 143 nm, whereas the Gd^{3+} $^8S_{7/2} \rightarrow {}^6D_J$ transition is excited at 252 nm in Fig. 9(b). The two spectra, normalized at the maximum of the $^3P_0$ emission line at 345 nm, are largely the same except for an enhanced Tm^{3+} $^3H_4 \rightarrow {}^3H_6$ emission under $Tm^{3+}5d$ excitation. This enhanced $^3H_4$ emission can be explained by the two successive cross-relaxation steps from Gd^{3+} to the $^3H_4$ state of Tm^{3+}, which were described above. The first step is cross relaxation between Gd^{3+} and Tm^{3+} involving the transitions $^6G_{7/2} \rightarrow {}^6I_J$ on Gd^{3+} and $^3H_6 \rightarrow {}^3H_4$ excitation of Tm^{3+} [see Fig. 10(b1)]. This cross relaxation results in the first excited Tm^{3+} ion in the $^3H_4$ state. In the second step, energy is transferred from the $^6D_{3/2}$ and $^6I_{3/2}$ states of Gd^{3+} to the $^3P_0$ state of Tm^{3+}, as indicated by the horizontal arrow in Fig. 10(b2). This transfer process can result in excitation of a second Tm^{3+} ion in the $^3H_4$ state after $^3P_0 \rightarrow {}^3H_4$ emission, as indicated in Fig. 10(b2).

The weak Tm^{3+} $^3P_0$, $^1D_2$, and $^3H_4$ emissions, as shown in Fig. 8(b) (the latter emission caused by radiative feeding from the $^3P_0$ state), compared to the Gd^{3+} $^6P_{3/2}$ emission are caused by a far more efficient nonradiative relaxation on Gd^{3+} from the $^6I_{3/2}$ and $^6D_{3/2}$ states to the $^6P_{3/2}$ state compared to energy transfer from Gd^{3+} to the $^3P_0$ state of Tm^{3+}. It must, however, be noted that the cross-relaxation step from the $^6G_{7/2}$ step to the $^3H_4$ and $^3H_5$ states [Fig. 10(b1)] predicts an equally intense Gd^{3+} $^6P_{3/2}$ emission compared to Tm^{3+} $^3H_4$ and $^3H_5$ emissions. Since only weak $^3H_4$ emission is observed, it must be concluded that cross relaxation mainly involves the $^3H_5$ state that has emission around 1250 nm which is outside the sensitive area of our CCD detector.

IV. CONCLUSIONS

VUV to IR luminescence excitation and emission measurements have revealed in detail how energy relaxes back to the ground state via complex energy transfer and emission scenarios after VUV excitation into the $5d$ states of Nd^{3+} and Tm^{3+} in $NaGdF_4$. In both systems, quantum splitting is observed that can result in the emission of two IR photons for each absorbed VUV photon.

Nd^{3+} $4f^25d^1 \rightarrow 4f^3$ emission in $NaLaF_4$:2% Nd^{3+} is quenched in $NaGdF_4$ by an identified cross-relaxation process involving the transitions $4f^25d^1 \rightarrow 4f^3$ (^4G_J) on Nd^{3+} and $^8S_{7/2} \rightarrow {}^6D_J$ on Gd^{3+}. This results in Nd^{3+} emission from the $^4F_{3/2}$ state in the IR after nonradiative relaxation from the ^4G_J state. A second photon from the $^4F_{3/2}$ state of Nd^{3+} can be emitted after Gd^{3+} ($^6P_{3/2}$) $\rightarrow Nd^{3+}$ ($^2H_{9/2}$) energy transfer followed by Nd^{3+} $^2H_{9/2} \rightarrow {}^4D_{3/2}$ nonradiative relaxation and Nd^{3+} $^4D_{3/2} \rightarrow {}^4F_{3/2}$ emission. Direct excitation of the Gd^{3+} $^6G_{7/2}$ state in $NaGdF_4$:2% Nd^{3+} results in quantum splitting through down-conversion as described recently by Jia *et al.*[10] in $LiGdF_4$:Nd^{3+}.

Tm^{3+} $4f^{11}5d^1 \rightarrow 4f^{12}$ emission in $NaLaF_4$:Tm^{3+} is quenched in $NaGdF_4$ by cross relaxation involving the spin-allowed and spin-forbidden $4f^{11}5d^1 \rightarrow 4f^{12}$ ($^3H_6$, $^3F_4$) transitions on Tm^{3+} and the $^8S_{7/2} \rightarrow {}^6G_J$ transitions on Gd^{3+}. This cross-relaxation step results in weak IR Tm^{3+} emission from the $^3H_4$ and $^3H_5$ states and strong Gd^{3+} $^3P_{3/2}$ emission. After cross relaxation, a small fraction of energy is transferred from the ^6D_J and ^6I_J states of Gd^{3+} to the $^3P_0$ state of Tm^{3+} which is followed by Tm^{3+} $^3P_0 \rightarrow {}^3H_4$ emission and successive $^3H_4 \rightarrow {}^3H_6$ emission. In this case, three photons are emitted for one absorbed VUV photon.

[1] R. T. Wegh, H. Donker, K. D. Oskam, and A. Meijerink, Science **283**, 663 (1999).
[2] R. T. Wegh, H. Donker, E. van Loef, K. D. Oskam, and A. Meijerink, J. Lumin. **87**, 1017 (2000).
[3] W. M. Yen, S. Shionoya, and H. Yamamoto, *Phosphor Handbook* (CRC, Boca Raton, FL, 2006).
[4] T. Trupke, M. A. Green, and P. Wurfel, J. Appl. Phys. **92**, 1668 (2002).
[5] C. R. Ronda, J. Alloys Compd. **225**, 534 (1995).
[6] T. Jüstel, H. Nikol, and C. R. Ronda, Angew. Chem., Int. Ed. **37**, 3085 (1998).
[7] C. Feldmann, T. Jüstel, C. R. Ronda, and D. U. Wiechert, J. Lumin. **92**, 245 (2001).
[8] V. Babin, K. D. Oskam, P. Vergeer, and A. Meijerink, Radiat. Meas. **38**, 767 (2004).
[9] P. S. Peijzel, W. J. M. Schrama, and A. Meijerink, Mol. Phys. **102**, 1285 (2004).
[10] W. Jia, Y. Zhou, S. P. Feofilov, R. S. Meltzer, J. Y. Jeong, and D. Keszler, Phys. Rev. B **72**, 075114 (2005).
[11] J. H. Burns, Inorg. Chem. **4**, 881 (1965).
[12] A. Aebischer, M. Hostettler, J. Hauser, K. W. Krämer, T. Weber, H. U. Güdel, and H. B. Bürgi, Angew. Chem., Int. Ed. **45**, 2802 (2006).
[13] K. W. Krämer, D. Biner, G. Frei, H. U. Güdel, M. P. Hehlen, and S. R. Lüthi, Chem. Mater. **16**, 1244 (2004).
[14] G. Zimmerer, Nucl. Instrum. Methods Phys. Res. A **308**, 178 (1991).
[15] R. T. Wegh, W. van Klinken, and A. Meijerink, Phys. Rev. B **64**, 045115 (2001).
[16] P. W. Dooley, J. Thogerson, J. D. Gill, H. K. Haugen, and R. L. Brooks, Opt. Commun. **183**, 451 (2000).
[17] P. S. Peijzel, P. Vergeer, A. Meijerink, M. F. Reid, L. A. Boatner, and G. W. Burdick, Phys. Rev. B **71**, 045116 (2005).